Laser and Particle Beams (2001), *19*, 295–308. Printed in the USA.

Studies on nonconventional high-gain target design for ICF

A. CARUSO AND C. STRANGIO

Associazione EURATOM-ENEA sulla Fusione, C.R. ENEA Frascati, Via E. Fermi 45, 00044 Frascati (RM), Italy

(RECEIVED 19 July 2000; ACCEPTED 9 December 2000)

Abstract

This paper reports some of the studies on nonconventional ICF approaches performed at the ICF Physics and Technology Laboratory of the AEEF in Frascati, Italy. Having as reference potential difficulties associated to the conventional central spark ignition (fuel mixing) and to the usual approach to fast ignition by laser (transfer and coupling of the energy pulse, fast electrons energy tuning), we have made explorative work on possible alternatives. The performances of targets ignited near stagnation by pulses of heavy ion beams (HIB) or by macroparticle impact were previously studied. The needed driver energy, the power, and the beam quality requirements, as well as the level of synchronization the implosion and the igniting pulse have been found. More recently, to relax some requirements on the HIB beam parameters set by the previous approach, the injected entropy approach (IE) has been introduced. In this method, the conditions for spark formation are set in the final stages of the implosion, when the spark fuel size is a few times the final size at stagnation (volume a few tens of the final). Energy is injected at this time to set the spark fuel on a high adiabat. In this paper, for illustration and comparison purposes, some relevant results we previously obtained for near-stagnation ignition are first introduced and critically reviewed. The new IE method, after a short analytical introduction, is presented and illustrated by the results of extensive 2-D numerical simulations. The considered cases refer to imploding cylinders of finite length. As required by this approach, one or two opposing beams axially injected additional energy, whereas the acceleration stage of the cylindrical low-entropy implosion was assumed driven by a different driver. Heavy ion beams, soft X-rays (SXR), and laser generated light ion beams were considered as vectors for the entropy injection. Issues related to the feasibility of these generators are discussed. The study was made for various initial conditions leading to different ignition modes and burn propagation. The most recent results on the injected entropy method to the ignition of high gain targets are included.

Keywords: Cylindrical implosions; Inertial confinement; Heavy ion beams; Light ion beams; X-rays

1. INTRODUCTION

In the extensively more studied ICF scheme, to get thermonuclear ignition in the laboratory, the ignition spark is self-formed at the center of a compressed fuel, at the end of an implosion process. A properly tailored hydrodynamic process sets the inner layers of an imploding fuel capsule on a high adiabat to produce the spark. The mass of the spark is much smaller than that of the surrounding cold and dense fuel (a few percent) which, for high gain, ought to be compressed along a lower adiabat (Nuckolls *et al.*, 1972; Afanasiev *et al.*, 1975).

In the fast ignition approach, the fuel is entirely compressed along a low adiabat, and the spark is generated at stagnation, near the fuel assembly boundary, by a short laser or heavy-ion pulse. In this way, the entire ignition spark energy is provided by a dedicated, additional driver (Basov *et al.*, 1992; Caruso, 1994; Caruso & Pais, 1996; Tabak *et al.*, 1994).

Main issues for these two approaches may be the following. The central spark approach is based on the use of a single high-power system used to drive a quite sophisticated implosive process in a spherical thin shell (typically *shell radius/shell thickness* ≈ 30). All the premises for the spark formation are determined during this acceleration process, developing along $\frac{1}{3}$–$\frac{1}{2}$ of the initial shell radius. During this process, the inner layers of the shell (the future spark material, a few percent of the shell thickness) are set on a comparatively higher adiabat by a sequence of shocks. All the subsequent evolution is imprinted during this stage, corresponding to geometrical and physical conditions very re-

Address correspondence and reprint requests to: A. Caruso, CRE ENEA Frascati, Via E. Fermi 45, 00044 Frascati (RM) Italy. E-mail: caruso@frascati.enea.it

mote from the final, aimed ones. Large excursions feature all the geometrical and physical parameters along the way to get ignition conditions (typically, *initial fuel shell radius/spark radius* $\approx 40-60$, fuel density ratio > 1000, etc.). In this scenario featured by high convergence hydrodynamics, the possibility of influencing the final stages of the compression by an external additional intervention is not considered. Very relevant issues, in this scheme, are the uniformity of energy deposition on the capsule and the effects of hydrodynamic instabilities. One of the currently considered processes that may lead to the ignition failure is the final mixing of the high isentrope fuel with the low isentrope one, due to instabilities seeded by initial small perturbations imprinting. High gain with mixing may be recovered for target designs leading to comparatively higher final densities (as $\times 2$–3, see Caruso & Strangio, 1998).

The fast ignition approach requires two drivers, one to drive a low adiabat implosion (and get a dense fuel assembly), the other to create the hot spark on the compressed fuel surface. For this approach the role of the hydrodynamic instabilities could be less relevant since, for example, fuel mixing processes in the final stages of the implosion, if active, will be ineffective. However, transfer of the trigger energy to the compressed fuel and the formation of a properly sized spark may be a real issue. Two drivers have been proposed for spark injection, namely lasers operated in the ultrashort pulse mode (e.g., picosecond pulses; Tabak *et al.*, 1994), and ultrabright heavy ion pulses (HIB; see Caruso, 1994).

Lasers operating in the ultrashort mode are currently used, and deliver sizable energies (several hundreds of Joules) in laser-matter interaction experiments at high power densities ($>10^{19}$ W/cm^2). However, for the application of short pulses to the formation of an ignition spark, several physical issues have to be favorably solved, and mastering a complex chain of processes will be necessary. The detailed list of the events involved is quite long, but can be split into two basic categories.

The first category refers to the channeling of the igniting pulse through the remnants of the ablation process used to drive the fuel compression. These remnants are formed by supercritical plasma (imaginary refraction index for the light pulse) and undercritical plasma. The strategy proposed is to drill a channel through the corona by a preliminary laser pulse (by electrodynamic or heating processes), and then to inject in this channel another pulse, to generate the ignition spark by a burst of fast electrons.

As suggested by the following argument, the second category of problems refers to the formation of the properly dimensioned ignition spark by the fast electrons produced by the heating pulse. The power flux I required for ignition results determined as a function of the fuel density ρ and the spark temperature T ($I \propto \rho T^{3/2}$). The required T being more or less given (about 10 keV), it follows that to each ρ corresponds a value of I and of the fast electron energy and range. Clearly the fast electron range results are matched to the optimal spark size (≈ 0.3 g/cm^2) only for a specific value of ρ and for a corresponding value of I. Being to some extent ρ assigned, the same will be needed for the ignition energy. For the propagation of the igniting pulse, this level of control implies the success in producing a channel completely plasma free. Otherwise self-focusing in subchannels will result in a spread for the local values of I and in a corresponding spread for the fast electrons energy and range.

We performed studies for the fast ignition by HIB and macroparticle (MP) impact (see Caruso, 1994; Caruso & Pais, 1996, 1998). These energy vectors have been selected because no substantial target coupling issues are expected. By extensive numerical 2-D simulations, the requirements to have ignition and high gain have been calculated for energy/power, focusing, and timing. As targets for the HIB, static fuel assemblies (ignition threshold calculations) and laser imploding targets (ignition, gain, and synchronization studies) were considered. From these studies, a relationship between the focal spot radius and the associated trigger energy/power was obtained. For this approach a major technical problem seems to be the production of highly space-time compressed HIB. Following a model used in this paper (Sect. 4), using the above-mentioned data, the required unnormalized beam emittance can be estimated as a function of the beam neutralization. Typical results are values ranging between 0.1 and 0.3 mm-mrad, for neutralizations greater than 0.9.

To relax some requirements on the driver parameters set by the HIB fast ignition, the injected entropy approach was introduced. This scheme is based on the energy injection in the final stages of the target implosion. Most of the energy needed to form the ignition spark is still provided by the work of the imploding target itself and the injected energy is used to set on a higher adiabat that small portion of the fuel destined to become the ignition spark.

Typically, a possibility could be the one in which the size of the hot spot created by energy injection is $\approx 3.5 \times$ final ignition spark size. Values for the fuel density where the energy is deposited could be $\rho \approx 1$ g/cm^3 and the temperature to be achieved $T \approx 1$ keV. Correspondingly $I \approx 4 \times 10^{15}$–$2 \times 10^{16}$ W/cm^2 follows.

Most of the energy is still being provided by compression work; this method is clearly similar to the conventional central spark approach, but with several potential advantages. A basic one is that the conditions for spark formation are set up when the physical conditions of the fuel assembly are not so remote from the aimed ones, as in the case of standard approach. Actually, the mentioned typical convergence ratio (3.5), taken since the time of energy injection, appears quite modest if compared with that typical of the standard approach, in which the spark fuel is mainly set on a high isentrope in the initial stages of the implosion process. Compared to the standard approach, another potential advantage of the method is that the main fuel can be compressed along a comparatively lower adiabat, the selection of the fuel to be set on the high adiabat being more precise

https://doi.org/10.1017/S0263034601192190 Published online by Cambridge University Press

(higher gain). With regard to high-to-low isentrope fuel mixing by instabilities, the formation of the high adiabat spot may cure hydrodynamic nonuniformity by internal ablative and mixing processes. Although speculative, all these are potentials introduced by the active intervention in the final stages of the implosion.

In this paper, the entropy injection method is first briefly introduced by a 0-D model, which allows the discussion of the different ignition strategies in the areal mass and temperature plane (density $\rho \times$ radius R, temperature T). To validate by a more complete physical description the feasibility of the approach, numerical 2-D simulations were performed to study the injected energy transfer to the matter destined to become the ignition spark, the final stages of compression (by the surrounding denser fuel), and the ignition burn process. Finite length imploding cylinders have been chosen as targets. Heavy-ion beams (HIB), soft X-rays (SXR), and light ion beams (LIB) were considered as vectors for the entropy injection. Some evaluations to frame the performances required for these generators will be also presented.

Cylinders were selected as targets because of the injection possibility along the axis. These configurations are also especially promising for high-gain designs because of the possibility of radial implosion velocity tailoring along the cylinder axis. Based on this possibility, the region where the ignition starts can be made (e.g.) to implode at higher velocity than the remaining main fuel, which is the payload in the scheme. This flexibility seems absent in spherical geometry.

Finally it was demonstrated that a class of implosion designs having similar performances in terms of gain, hydrodynamics, driver and α-particle transport can be deduced by simple analytical scaling laws.

In the simulations presented in this work, the 2-D codes CoBi and its evolution COBRA were used. Both these codes have been developed at the Inertial Physics and Technology Laboratory (ENEA CR Frascati). Their main features are:

- both the codes are Lagrangian;
- the physical model is based on a three temperature description (ionic temperature, electronic temperature, radiation temperature);
- finite range for the α-particle;
- the EOS and the opacity coefficients are given by models producing values in agreement, for the published cases, with those reported in the SESAME tables (Los Alamos EOS and Opacity Group 1983);
- the HIB deposition is described by models as those reported in Mehlhorn (1981) and Brueckner *et al.* (1982) (with modifications to fit some experimental data existing for range in cold matter);
- the X-ray driver beam is propagated by angular and frequency multigroup ray tracing, in which geometrical optics was included (i.e., refraction);
- a collision method is used to avoid extreme mesh distortion (see Pais & Caruso, 1990).

2. FAST IGNITION BY HEAVY IONS OR MACROPARTICLE IMPACT

In this section we summarize a study in which the dependence of the trigger energy on focusing is first analyzed for compressed, static equimolar DT fuel. Cold DT cylinders at a density of 200 g/cm^3 (and diameter substantially greater than the heavy ion spot) were assumed to be coaxially irradiated by a 15-GeV Bismuth HIB of energy $E_{trigger}$. A modified Gaussian profile was adopted for the power time-dependence, τ_{pulse} being the typical FWHM duration.

For the HIB space distribution, a cylindrical geometry, coaxially impinging onto the irradiated targets, was adopted. The ion beam radial distribution was taken to be a Gaussian characterized by a beam diameter d_{beam} (d_{beam} = diameter at $1/e$ of maximum power density). The beam was truncated at $2 \times d_{beam}$ (that is at $1/e^4$ of maximum power density). The energy content within d_{beam} results in about 64% of the total.

The useful time for the ignition spark formation at the assumed fuel density is about 20 ps, which is about the ratio between the initial heavy ion range and the sound velocity evaluated at the ignition temperature (5–7 keV). For shorter pulse duration, the energy transferred to the target is the main parameter, whereas for longer pulses, the relevant one is the beam power. Thus, we ran 2-D numerical simulations for pulse duration $\tau_{pulse} = 10$ ps or $\tau_{pulse} = 50$ ps, to study these different regimes.

The results of the simulations are summarized in Figure 1. Although $E_{trigger}$ is different for the two pulse durations, the qualitative behavior results are the same. For both cases, the smallest ignition energy (E_{min}) is constant for spot radii

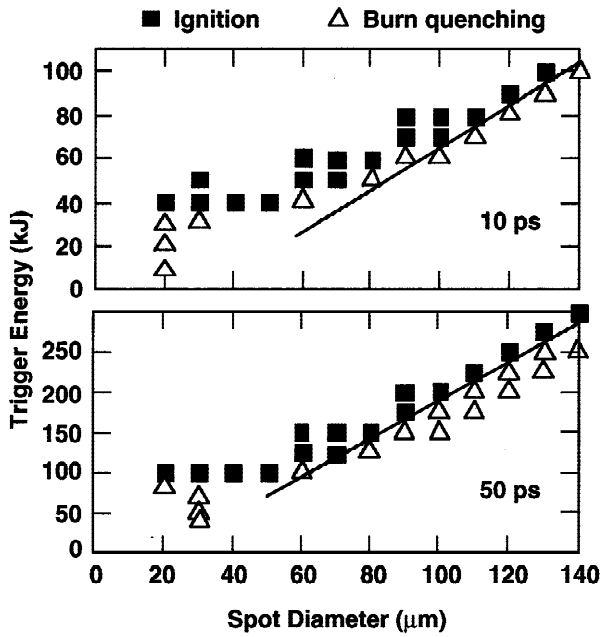

Fig. 1. Energy needed to ignite static cylinders of equimolar DT at 200 g/cm^3. The energy is given as a function of the spot diameter for two values of the pulse duration.

https://doi.org/10.1017/S0263034601192190 Published online by Cambridge University Press

smaller than 50 μm. In the range 50–140 μm, the ignition energy increases almost linearly ($3 \times E_{min}$ at 140 μm, with $E_{min} = 40$ kJ for 10 ps pulses, $E_{min} = 100$ kJ for 50 ps pulses). At any rate, a minimum trigger energy results from these studies, namely

$$E_{trigger} = 40 \times \left(\frac{200}{\rho}\right)^2 \text{ kJ.} \quad (1)$$

Trigger conditions and achievable gain have been studied for the case of HIB-started ignition in laser irradiated targets imploding along a low isentrope. The same situation was also used to study the degree of synchronization needed to get high gain (high-gain window).

The imploding capsule data have been taken from 1-D calculations and given as initial conditions to the 2-D code, when the HIB irradiation was started. The space-time distribution of the HIB was the same used in the static cylinder studies, but the 50-ps duration was adopted. General features of the cold implosion design were the following.

The target was a DT spherical shell with aspect ratio (*radius*/*thickness*) set to 10. The laser pulse energy was 1 MJ at $\lambda = 0.35$ μm. To minimize the energy stored in the compressed fuel, the first shock driven in the fuel was relatively weak, to keep the implosion on a low adiabat. A long ($\approx$100 ns) low-power forerunner, anticipating the main high-power peak characterized the laser pulse. Pulse time shaping was such that *forerunner duration*/*high-power pulse duration* ≈ 10 and the *forerunner energy* $\approx 10\%$ of the total. The maximum implosion velocity was $V_{max} \approx 1.3 \times 10^7$ cm/s. At stagnation, the fuel remained for an unusually long time at high density, its specific internal energy being nearly that of a cold material (low sound speed). These results are relevant in connection with the synchronization issues.

The results of the simulations are shown in Figure 2. Changing the timing for the same trigger pulse parameters, it is possible to find the time window in which ignition and high burn occurs. A relatively long temporal window of 720 ps around the stagnation point exists. In this window the total fusion energy release exceeds 300 MJ. Considering the energy invested in compression (1 MJ) and ignition (100 kJ), it leads to an overall energy gain in excess of 270 (gain = *thermonuclear energy*/(*laser energy* + *trigger energy*)).

Two different evolutions can be noted. For spot diameters below 70 μm, the window length (defined as the interval in which the thermonuclear yield is greater than 300 MJ) decreases when d_{beam} increases (from 720 ps to 520 ps). For $d_{beam} \geq 70$ μm ($E_{trigger} = 150$ kJ), the window starts to increase, reaching 920 ps at $d_{beam} = 100$ μm ($E_{trigger} = 225$ kJ). For $d_{beam} = 150$ μm ($E_{trigger} = 375$ kJ) a central hole is generated in the window.

From the data in Figure 2 (d_{beam}, $E_{trigger}$) the dependence of $E_{trigger}$ on d_{beam}, can be found. The result is

$$E_{trigger} = 91.3 + 0.013 d_{beam}^2, \quad (2)$$

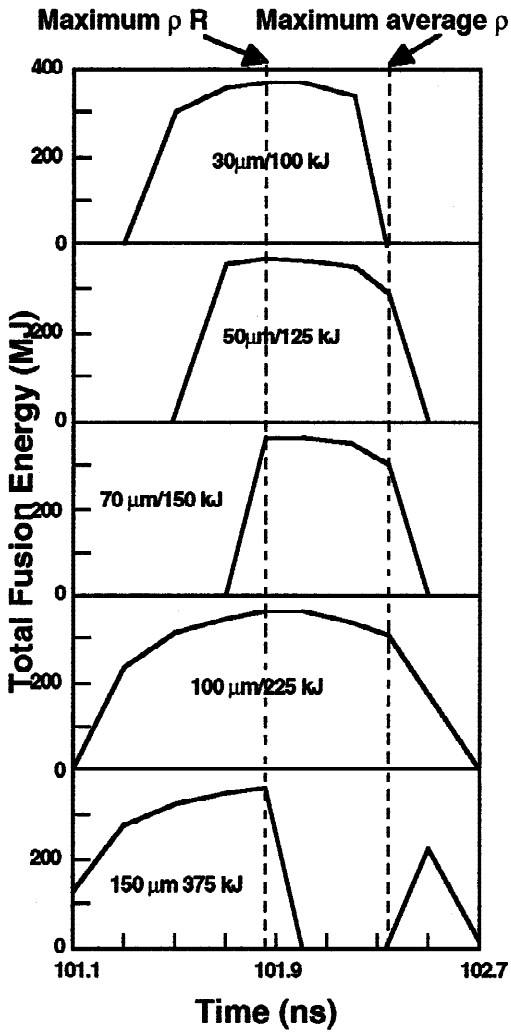

Fig. 2. Ignition windows as a function of the focal spot dimensions. The energy displayed in the frames is the minimum value needed to get ignition at the maximum ρR time. The HIB duration was 50 ps FWHM.

where $E_{trigger}$ is in kiloJoules and d_{beam} in microns. Equation 2 is valid in the range 30–150 μm and is useful to evaluate the beam current as a function of the spot diameter and to explore the beam quality requirements. For instance, by using Eq. 2, taking into account space charge effects (at level of envelope description, see Sect. 4) and chromatic aberrations, it is possible to find preliminary information about the beam emittance and the degree of required neutralization. It is found that the beam unnormalized emittance at the focusing lens has to be less than 0.3 mrad-mm (corresponding, in typical reactor dimensioning, to a transverse momentum spread $dp_\perp/p_\perp \approx 4 \times 10^{-6}$). Following the model used in this paper (Sect. 4), the longitudinal momentum spread $dp_\parallel/p_\parallel$ has to be kept less than 10^{-5} and the neutralization has to be greater than 0.9. As multibeam operation will possibly be required, adequate aiming precision is necessary.

In Figure 3 is shown the ignition and burn for one of the cases considered for Figure 2. The maps refer to the case

https://doi.org/10.1017/S0263034601192190 Published online by Cambridge University Press

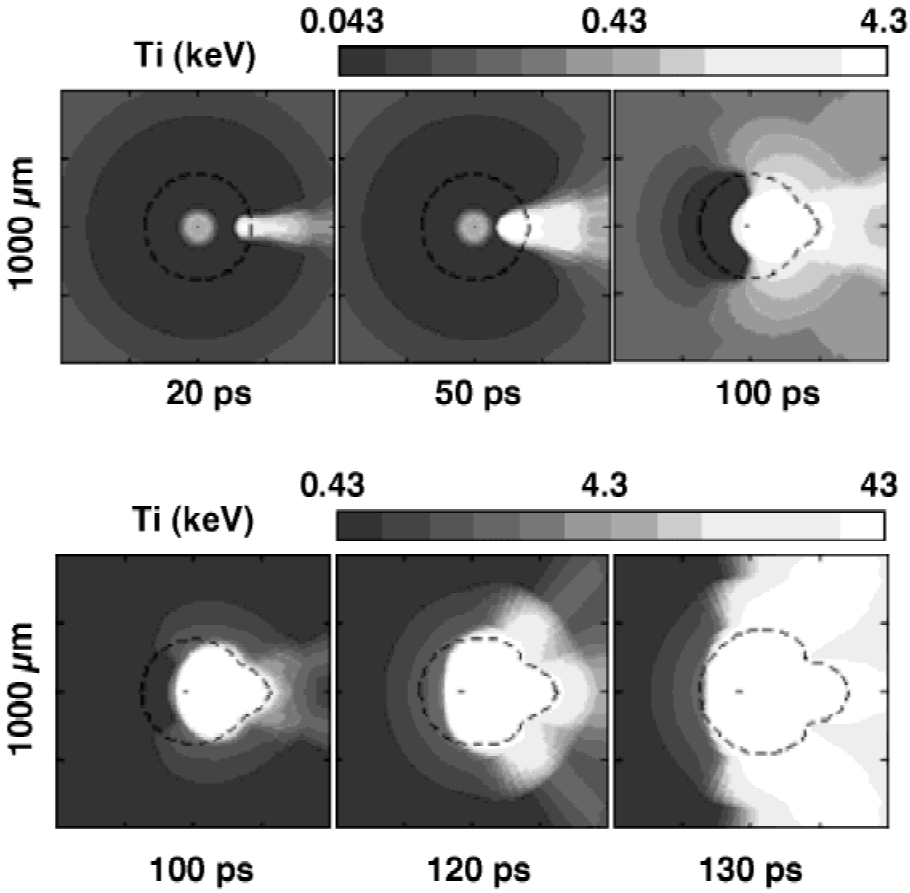

Fig. 3. Ionic temperature maps for the ignition and burn of a spherically laser-compressed fuel. The dashed circle limits the high-density fuel region, the corona remnant being distributed outside. The overall energy gain exceeds 270.

shown in the top of Figure 2, and the synchronization is for HIB starting at the time of maximum ρR.

In the impact of a high-Z MP moving at $4-6 \times 10^8$ cm/s with a high density DT fuel (say 200 g/cm^3), the dominating physical process is the radiative collapse of the macro particle on the fuel surface (Caruso, 1994; Caruso & Pais, 1996). A large fraction of the shocked MP internal energy is lost in radiation waves moving at velocities of the order of 3×10^9 cm/s, one rising upstream of the collapsing particle, the other forerunning, downstream, the shock wave in the DT fuel. The typical radiation temperatures are of the order a few kiloelectronvolts (3–4 keV). Due to these losses, the MP collapses to very high densities ($>10^3$ g/cm^3), whereas the matter temperature (ions and electrons) is brought to equilibrium with the radiation temperature. Due to this process, regardless of its initial shape, the MP is reduced to a very thin layer on the DT fuel (a fraction of microns). However, since the momentum is conserved, a well-defined fraction of the energy remains in the matter. A sufficiently accurate quantitative description of the relevant processes is obtained by a snow-plough model where the internal energy in the shocked projectile is assumed negligible and its density infinite (*internal energy per unit surface* $\approx$ *finite pressure* $\times$ *vanishing thickness*). To close the system, it is assumed that the fuel is passed by a strong shock wave producing a compression ratio of 4. The governing parameter in this process is $a = (4\rho_{DT}/3\rho_{MP})^{1/2}$, where ρ_{DT}, ρ_{MP} are the fuel and the MP densities. As a function of a and ϵ (the specific internal energy transferred to the fuel), we find the shock velocity in the fuel $D = 2(2\epsilon)^{1/2}$, for the projectile velocity $V_{MP} = (1 + a)(2\epsilon)^{1/2}$ and for the shocked fuel velocity $V = (2\epsilon)^{1/2}$. If to ϵ is assigned the value needed to get ignition (about 6.8×10^{15} erg/g at 5 keV), all these velocities are determined. This model was used to find an estimate for the trigger energy and for the dimensioning of 1-D and 2-D simulations.

In the 2-D simulations, the impact of a gold cylinder 40 μm long and 40 μm in diameter on a DT half-space at a density 200 g/cm^3 was considered. No ignition occurs at MP velocity 4×10^8 cm/s. Ignition is recovered by raising the velocity to 5×10^8 cm/s. This velocity corresponds to a threshold energy of about 12 kJ (MP mass of 0.97 μg). This case was used to normalize a theoretical formula for the ignition energy:

https://doi.org/10.1017/S0263034601192190 Published online by Cambridge University Press

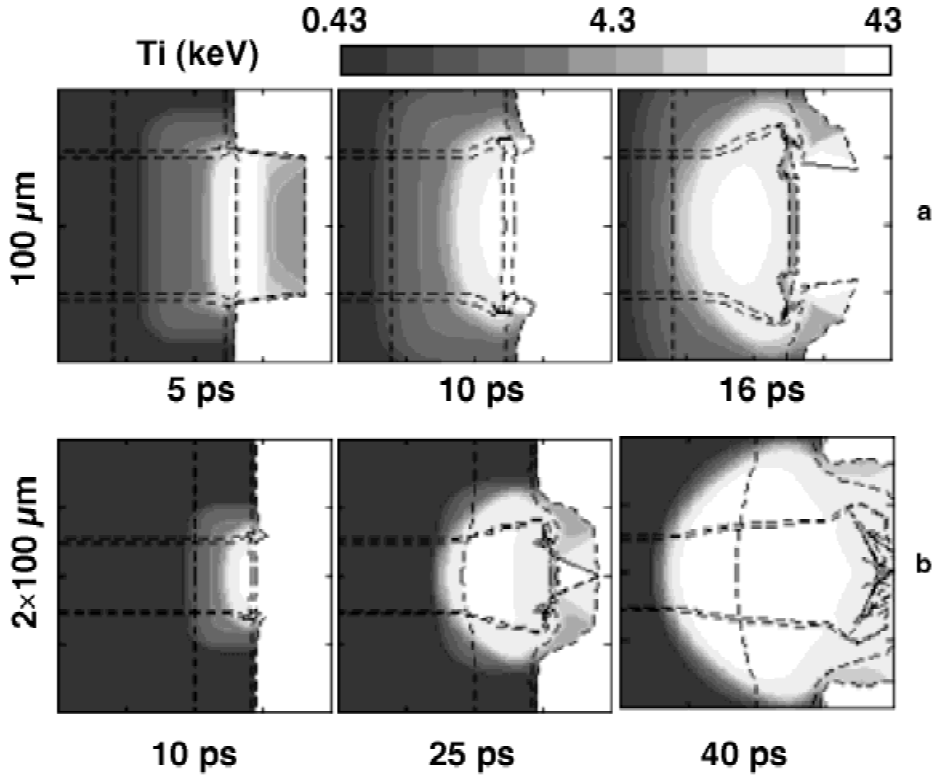

Fig. 4. Ignition by macroparticle impact. A gold cylinder (diameter and length 50 μm, velocity 6×10^8 cm/s) collides with a 200 g/cm^3 DT half space. Ion temperature maps. (a) Initial interaction stages (100 μm $\times$ 100 μm field); (b) Evolution of the ignition process (200 μm $\times$ 200 μm field).

$$E_{trigger} = 3.5 \times 10^3 a(1+a)^2 \frac{1}{\rho_{DT}^2} \text{ kJ}. \quad (3)$$

An example of ignition by MP impact is shown in Figure 4.

In conclusion, for the fast ignition of a DT fuel at 200 g/cm^3 by impact of a dense solid MP, energies around 10 kJ ought to be associated to masses of the order of 1 μg.

3. THE INJECTED ENTROPY APPROACH

Models of 0-D have been widely used for approximate treatments of the final stages fuel destined to become the ignition spark (Kirkpatrick, 1979; Kirkpatrick & Wheeler, 1981; Lindl, 1995). We adopted the one described by the equation

$$\rho C_v \frac{dT}{dt} = W + P_\alpha - H - P_r, \quad (4)$$

where T is the temperature, ρ the mass density, C_v the specific heat at constant volume, t the time, P_α the energy locally released by the α-particles, H the losses due to electronic thermal conduction, P_r the radiative losses and W the work exerted by the rest of the fuel. W is calculated following a kinematics that includes the implosion slowing down and a turn-around point near stagnation, and P_r is evaluated according to a model that includes radiation trapping (Caruso & Strangio, 2000). The scenario for the spark fuel evolution arising from Eq. 4 is shown in Figure 5, where V_0 is the initial asymptotic implosion velocity in units of 10^7 cm/s

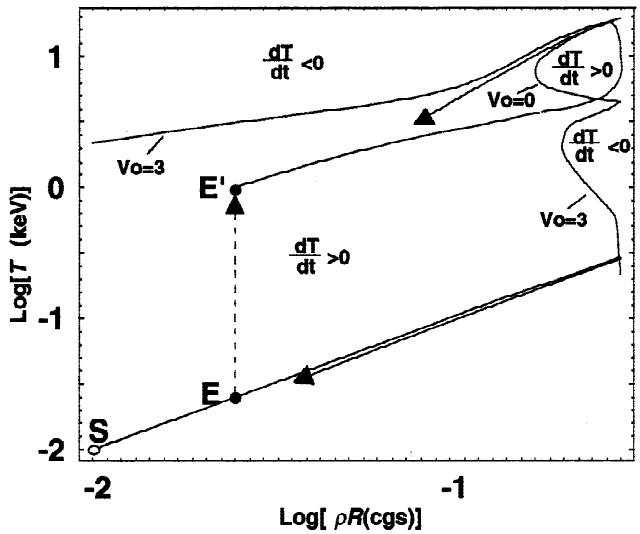

Fig. 5. In the IE scheme, the injection of energy results in a transition from a nonigniting implosion to an igniting one, from E to E′.

https://doi.org/10.1017/S0263034601192190 Published online by Cambridge University Press

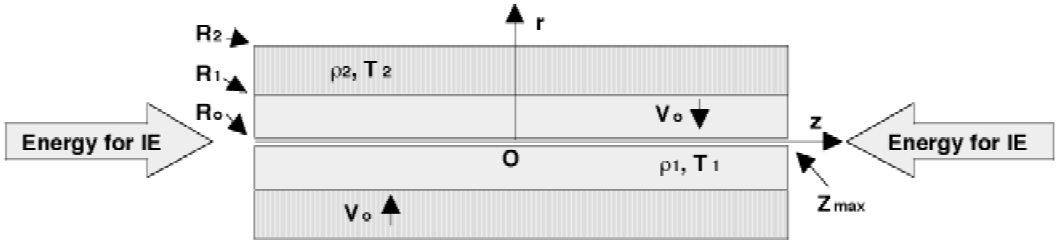

Fig. 6. A two macro-zone cylinder. The inner region (between R_0 and R_1) is filled by DT fuel at density $\rho_1 = 0.25$–1 g/cm^3, the outer layer (between R_1 and R_2) by DT at $\rho_2 = 50$ g/cm^3. Both these macro-zones are set imploding at velocity V_0 typically 2–3×10^7 cm/s.

and R is the spark material radius at the time t. For $V_0 = 0$, the work term is zero. In this case, the only region where the temperature increase is allowed is the one near the upper-right corner in Figure 5. For $V_0 = 3$ the region where the increase of temperature is possible becomes a continuous band connecting low to high temperatures. In this case, solutions to Eq. 4 that represent compression without ignition (e.g., the one starting from S) or compression with ignition (e.g., that traced from E′) can be found. A transition from a point E of a nonigniting solution to a point like E′ (staying on an igniting one) can be produced by injection of a short energy pulse that in Eq. 4 would appear as a δ-function. In this operation, the energy pulse sets the spark material on a high adiabat while the achieved temperature is much less than the final one needed for ignition. The energy transferred by the work of the remaining fuel along the solution starting from E′ brings the fuel to the ignition conditions. Typically, one possibility could be that the size of the hot spot created by energy injection is $\approx 3.5 \times$ final ignition spark size. Values for the fuel density where the energy is deposited could be $\rho \approx 1$ g/cm^3 and the temperature to be achieved $T \approx 1$ keV. Correspondingly it follows that $I = 2$–3×10^{16} W/cm^2.

A physical description of the approach much more complete than that featuring the 0-D description is used in the numerical 2-D simulations presented in the following. The studied processes were the injected energy transfer to the matter destined to become the ignition spark, the final stages of compression (by the surrounding denser fuel) and the burn process. HIB, SXR, and LIB were taken as vectors for the entropy injection along the axis of finite length cylinders. In Figure 6, the range of some typical target parameters is indicated. Others are $R_0 = 6$–10 μm, $R_1 = 250$–500 μm, $R_2 = 370$–570 μm, $Z_{max} = 800$ μm, $t_{pulse} = 40$–1000 ps. The outer dense region was set on a low adiabat, whereas the inner region the α-ratio was typically about two. These targets do not ignite without the additional energy injection.

The formation of a low-density, low-temperature region within an imploding shell is a common process. When the acceleration towards the center (or symmetry axis) ends because the ablation pressure is removed, an expansion wave starts from the inner surface of the imploding layer, producing a low-density fuel region. In the case of a finite cylinder, the axial length covered by the expansion is of the same order of magnitude as the thickness of the low-density region itself. This is because the low-density layer formation and the end-losses are both essentially due to expansion waves. With regard to the effects of the end losses, these generally may have a positive effect. This is related to a better spark axial trapping by the higher density layer closure, eased because of a lack of counterpressure. In addition, the formation of higher density ploughs improves the burn process.

In the most interesting cases, the calculation for gain evaluations has been extended to the stages of burn propagation and target disassembling. The display of different modes of burn propagation along the peculiar, tubular density structures formed during the cylindrical target implosion was also a result of these studies.

4. HIB-ASSISTED IGNITION

In the simulations for HIB ignition, two opposing Bismuth HIB have been injected along the symmetry axis of the system to set the central zone of the low-density region on a high isentrope, as sketched in Figure 6. In the considered cases, Bragg peaks and beam superposition was of some

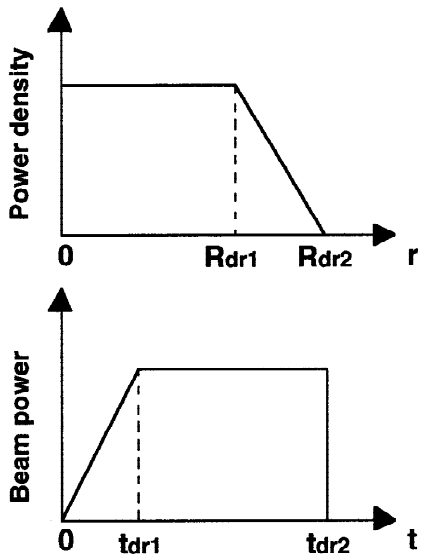

Fig. 7. Space and time dependencies for the HIB used in the simulations.

https://doi.org/10.1017/S0263034601192190 Published online by Cambridge University Press

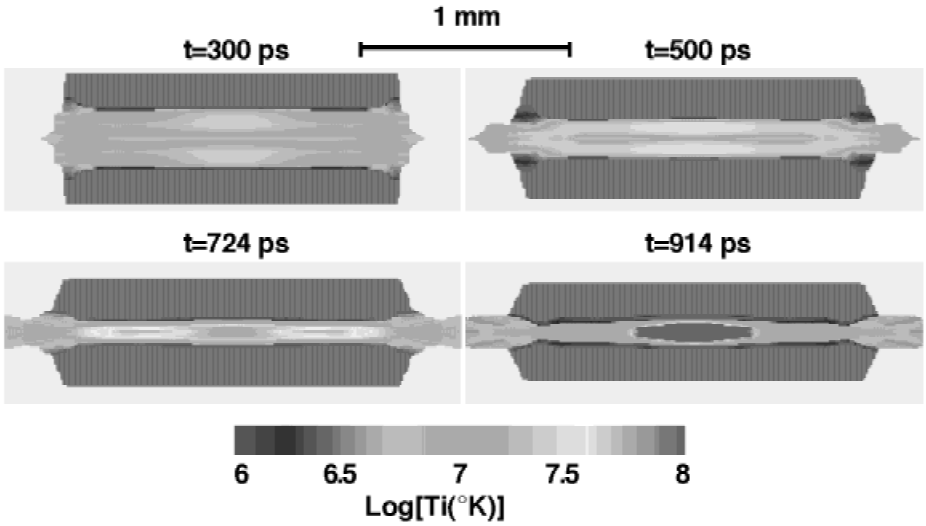

Fig. 8. Case 1 of Table 1. At the end of the HIB pulse (300 ps), the temperature in the central part of the target is raised to about 1 keV. Compression brings the same region to ignition.

importance for creating the conditions for ignition. Energy space and time distributions of beam were constant with linear space-time ramps (see Fig. 7). Typically, R_{dr2} was about 10% less than R_1 and the space-ramp length about 10% of R_1. The rise-time (t_{dr1}) was 16–30% of t_{dr2}.

In Figures 8 and 9 2-D maps for ionic temperature are shown for the case of Table 1. The yield for this kind of target is 2200–2400 MJ, corresponding to a *fuel-gain* of 2300–2500 (1330/mm). Typically the fractional burn result was about 0.4.

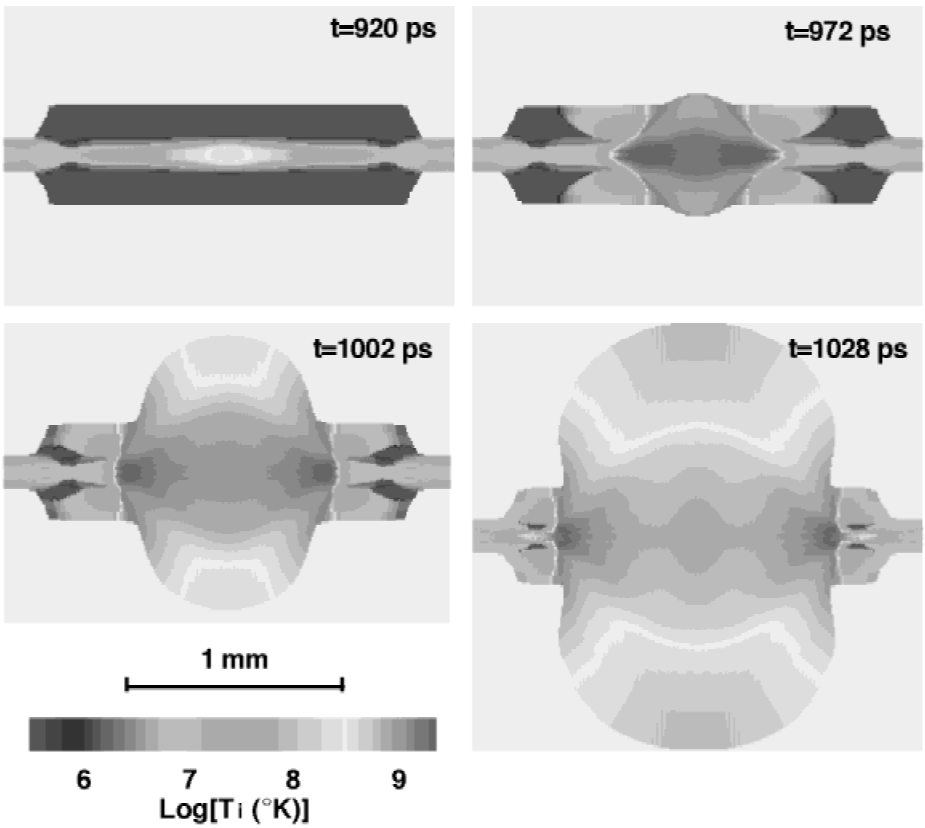

Fig. 9. Case 1 of Table 1, burn propagation. Two burn waves start from the center and propagate towards the cylinder open ends. Preheating to about the 1-keV level is due to radiation diffusion.

https://doi.org/10.1017/S0263034601192190 Published online by Cambridge University Press

Table 1. *System parameters*

Beam energy (kJ)	35
Ionic energy (GeV)	9.1
t_{HIB2} (ps)	300
R_1 (μm)	250
R_2 (μm)	370
ρ_1 (g/cm^3)	1
ρ_2 (g/cm^3)	50
$2z_{max}$ (μm)	1600
V_0 (cm/s) $\times 10^{-7}$	3
Ignition	Yes

Taking as reference the case of Table 1, let us consider a focusing from an initial radius of 7.5 cm on a spot of diameter $d_{HIB} = 0.5$ mm set at a distance of 5 m. The associated current is $I \approx 13$ kA $\approx I_{Maschke}$ (at 5 T). Contributions to the finite spot formation come from chromatic aberrations (d_{chr}) and emittance + space charge effects (d_{sc}). The total diameter can be estimated as

$$d_{HIB} = \sqrt{d_{chr}^2 + d^2}. \quad (5)$$

The envelope description (see Callahan & Langdon, 1996) was used to evaluate d_{sc} as function of the perveance and of the emittance. Some of the results for the case here considered are displayed in Figure 10. A possible usable situation is the one in which the neutralization is around 0.7. The associate beam quality is defined by a longitudinal spread in momentum $dp_{\|}/p \leq 1 \times 10^{-4}$ and an unnormalized emittance $\epsilon \leq 2.4$ mrad-mm (corresponding in our case to a transverse spread of $dp_{\perp}/p \leq 5 \times 10^{-5}$).

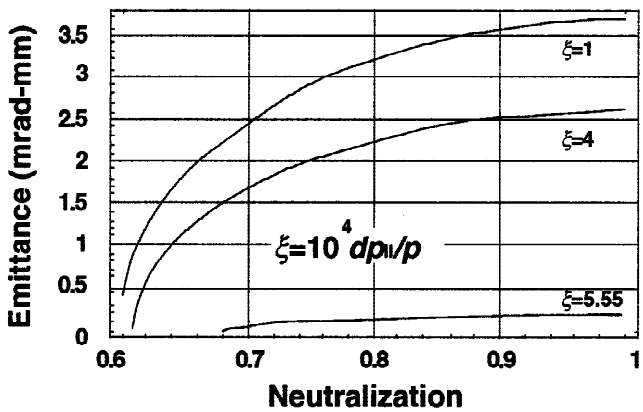

Fig. 10. Requirements on the HIB emittance at the focusing lens as a function of the beam neutralization. The quantity $dp_{\|}$ is the longitudinal momentum spread.

5. IGNITION ASSISTED BY NEAR TARGET SOURCES

A search was started to find near-target laser-produced sources adequate to start ignition in the IE mode. In the study, point-like emitters with assigned aperture were taken as virtual energy sources (see Fig. 11 for symbol definitions). A "cos(θ)" dependence was assumed for the power emitted in the unit solid angle. For assigned F/Number, different distances between the source and the cylinder, open end have been studied. Typically, beam diameters exactly matched that of the low-density region (i.e., $2R_1$). With respect to this configuration, the virtual source distance was in some cases reduced by Δ (see Fig. 11). Single as well two-sided irradiation has been studied. The power time dependence was the same as in Figure 7. As energy vectors, SXR and LIB were considered. Targets for one-sided irradiation were typically the same as those given in Table 1, with the total length reduced from 1.6 mm to 1.2 mm.

5.1. Ignition by SXR

Adequate coupling to get ignition in cylindrical targets (as those sketched in Fig. 6) can be obtained for soft X rays. In the simulations, the X-ray beam was divided in 8 photon energy groups and in 20 angular groups. Each group was

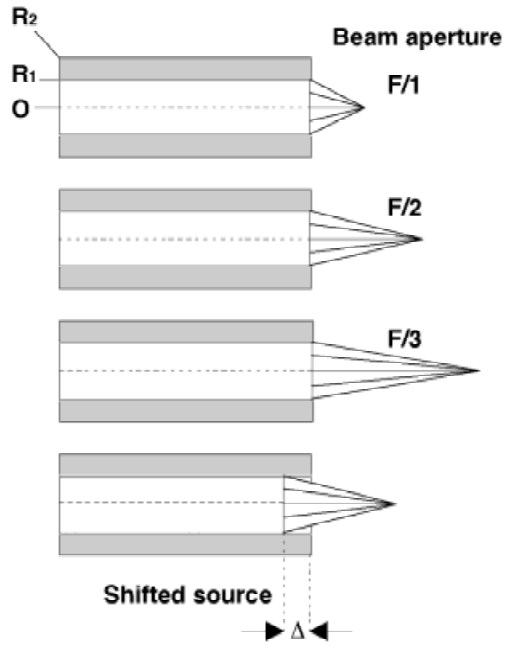

Fig. 11. Sources geometry used in the study for near target assisted ignition. Beam aperture (the F/Number) is defined by $\tan(\theta_{\max}) = 1/(2F)$, where $\theta_{\max}$ is the maximum angular semi-aperture of the beam.

https://doi.org/10.1017/S0263034601192190 Published online by Cambridge University Press

transported in the target according to a geometrical optics description including refraction and absorption (Caruso & Strangio, 1999).

The explored parameter space was the following

Energy	30–200 kJ
Implosion velocity	3×10^7 cm/s
Photon energy	60–2400 eV
SXR pulse duration	0.1–1 ns
Focusing	F/1, F/2, F/3
Source shift	$\Delta = R_1$

It was found that sources assembled by photons with energies in the range 200–900 eV can produce an ignition spark near the open ends. In this range of photon energies and in single-side irradiation mode, ignition and high burn were produced for apertures F/2 and F/3 at 80–100 kJ in 0.6 ns. No ignition occurred for F/1 in the same conditions. Ignition was earlier for F/2, but in the burn stage, F/3 surpassed F/2. Both F/2 and F/3 saturated to about the same level of burn. As a rule, by increasing the X-ray energy (e.g., in the range 100–200 kJ), ignition started earlier but burn saturated to a lower level. In Figures 12 and 13 are shown simulations in which the highest energy photon group used had 938 eV. The remaining seven groups were distributed between 63 and 813 eV, the most intense being those at 188, 313, and 438 eV, in a sort of bell-like distribution. Apart from the length, the target parameters were those displayed in Table 1. The performances of these targets are similar to those found for HIB-assisted ignition.

The source to be utilized for the previously described application cannot be Planckian. Actually, since power fluxes of the order of $2–3 \times 10^{16}$ W/cm^2 are needed, the temperature of such a source ought to be in the range 670–730 eV. Such a source is featured by a maximum of emission at 1900–2100 eV, a range of photon energy for which the coupling is not favorable. To assemble a source with proper spectral distribution, a nonequilibrium situation ought to be created on the frequency axis. Equilibrium to an appropriate "temperature" should be achieved within an intense absorption band of frequencies $h\nu < h\nu_{max} \approx 900$ eV, as sketched in Figure 14. As it is expected $T \gg h\nu_{max}$, it is possible to apply the Jeans distribution to find T as a function of the required flux ϕ .

$$T_{\mathrm{keV}} \approx 1.9 \times 10^{-16} \frac{\phi_{\mathrm{W/cm^2}}}{\nu^3_{\mathrm{keV}}} \tag{6}$$

For $\nu_{\mathrm{keV}} = 0.9$, $\phi = 2–3 \times 10^{16}$ W/cm^2 follows $T_{\mathrm{keV}} = 5–8$.

5.2. Ignition by LIB

Laser-generated LIB were considered for ignition in the IE approach. The assumed source positioning and aperture were similar to those adopted for SXR (see Fig. 11). Also the imploding target was the same. Pulses of deuterium ions at 6 MeV were considered. For aperture F/2, $\Delta = R_1$ and duration 40 ps, ignition and high burn were found for 20 kJ total energy. The short pulse duration adopted in this case was not strictly necessary for good coupling and derived from consideration on the LIB source. In Figure 15 the evolution of a target ignited by LIB in the IE mode is shown.

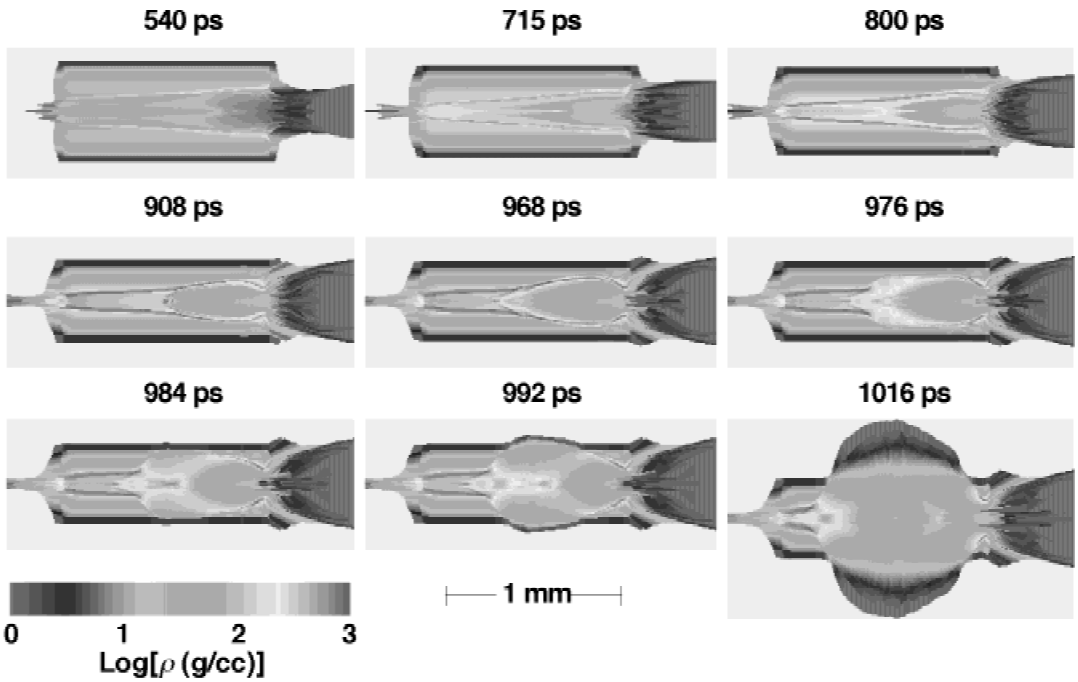

Fig. 12. Density maps during X-ray-triggered thermonuclear burn propagation.

https://doi.org/10.1017/S0263034601192190 Published online by Cambridge University Press

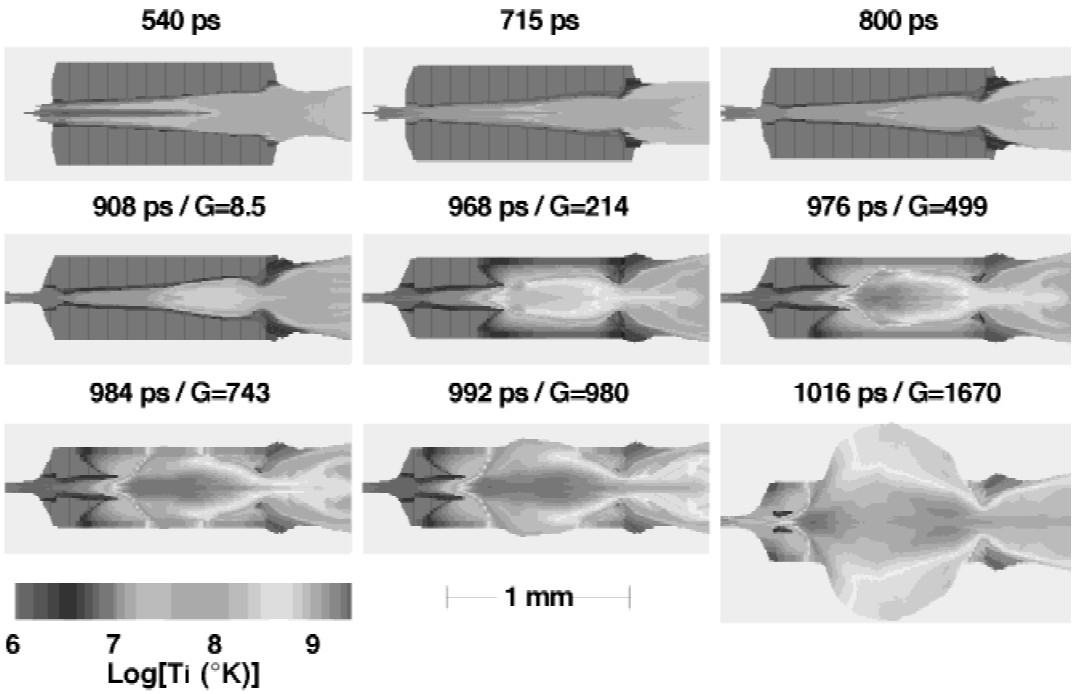

Fig. 13. Ionic temperature maps for burn propagation along an X-ray-ignited cylinder. G is the ratio between the released thermonuclear energy and the initial implosion energy.

Thin foils exploded by short laser pulses are natural candidates as sources of fast ions. This possibility was recognized early, when the first interaction experiments with ultrashort laser pulses were started (see Caruso & Gratton, 1971). The general idea is that if a finite fraction (η_{abs}) of the laser pulse energy is coupled to the electrons, energetic ion flow follows in the subsequent expansion, as the electronic pressure acts on the ions by electrostatic coupling (quasi-neutrality).

The time available for energy transfer from the laser to the electrons is limited by the plasma expansion, since at densities substantially lower than the critical (ρ_c) the system becomes transparent to the laser radiation. A conveniently dimensioned foil is that represented in Figure 16, where the initial and the exploded configuration are sketched. In this case, the initial thickness is chosen such that

$$Z_0 = \frac{\rho_c}{\rho_0} R_0, \tag{7}$$

where ρ_0 is the solid-state density (for solid deuterium and $\lambda = 1.054\ \mu$m, $\rho_0/\rho_c \approx 50$). When the plasma thickness becomes of the order of the diameter, the density is about ρ_c. At this time 3-D expansion becomes effective and makes the system rapidly transparent to the laser radiation. This occurs at the time

$$t_{int} \approx \frac{2R_0}{V_i}. \tag{8}$$

Here V_i is the final ion velocity (for deuterium ions at 6 MeV, $V_i \approx 2.4 \times 10^9$ cm/s). The time t_{int} represents the order of magnitude allowed for the laser pulse duration. Note that this time is substantially longer than the explosion time t_{expl}, since it is found that

$$t_{int} \approx \left(\frac{\rho_0}{\rho_c}\right)^{2/3} t_{expl} = \left(\frac{R_0}{Z_0}\right)^{2/3} t_{expl}. \tag{9}$$

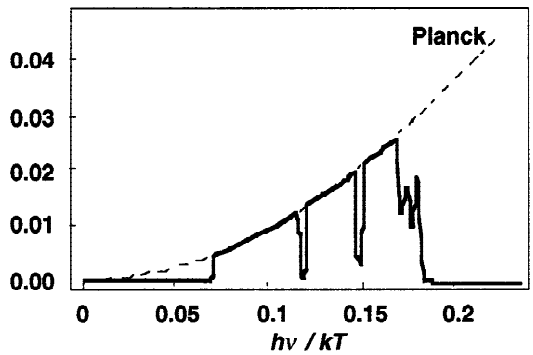

Fig. 14. A proper SXR source for application to IE would require a non-equilibrium state in which a low energy band is brought to a high "temperature" whereas the rest of the frequency axis is out of the equilibrium.

https://doi.org/10.1017/S0263034601192190 Published online by Cambridge University Press

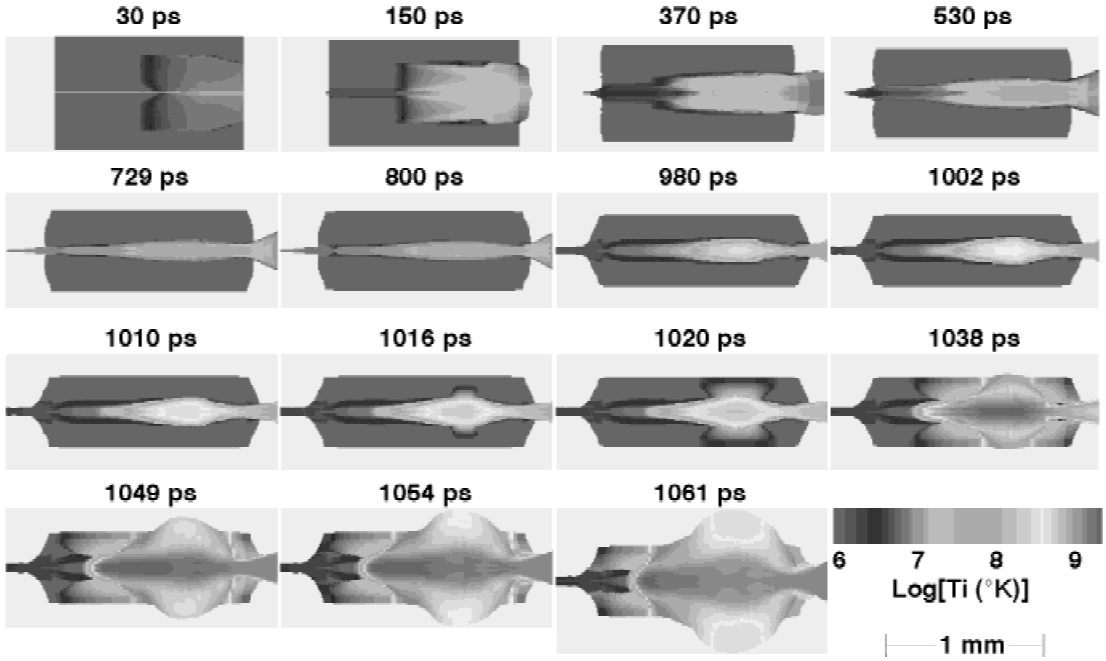

Fig. 15. Ionic temperature maps for a target ignited by 6 MeV deuterium LIB. The ignition and burn process starts from a well-trapped hot spark and propagates towards both the cylinder ends. The duration of the LIB pulse was 40 ps and the total energy 20 kJ.

The foil dimensioning can be given in terms of the total energy in the ion flow, E_{tot}. It is found:

$$R_0 = \left(\frac{E_{tot}}{\pi \rho_c V_i^2}\right)^{1/3} \propto \lambda^{2/3}, \qquad Z_0 = \frac{\rho_c}{\rho_0} R_0 \propto \lambda^{-4/3} \tag{10}$$

$$t_{int} \approx 2\left(\frac{1}{\pi}\frac{E_{tot}}{\rho_c V_i^5}\right)^{1/3} \propto \lambda^{2/3} \tag{11}$$

$$\phi_{abs} \approx \frac{1}{2}\rho_c V_i^3 \propto \lambda^{-2}. \tag{12}$$

In Eq. 12, ϕ_{abs} represents the power density to be absorbed on the target surface. The impinging flux would be $\phi = \phi_{abs}/\eta_{abs}$. Note that ϕ_{abs} do not depend on E_{tot}. Furthermore the only quantity depending on the initial solid density is Z_0. For $\lambda = 1.054$ μm, $\rho_0 = 0.169$ g/cm^3, and $E_{tot} = 50$ kJ, we get from Eqs. (10–12), $R_0 \approx 200$ μm, $2Z_0 \approx 10$ μm, $\phi_{abs}\lambda_\mu{}^2 \approx 3 \times 10^{18}$ W $\times$ μm^2/cm^2, $t_{int} =$ 20 ps. If the laser wavelength is decreased, the target aspect ratio $q = R_o/Z_0$ decreases, the power density increases, and the pulse duration decreases.

Let us assume $\eta_{abs} = 0.5$. From the previously considered dimensioning it follows that $\phi \times \lambda\mu^2 \approx 6 \times 10^{18}$ W $\times$ μm^2/cm^2 and a quiver electronic kinetic energy $K_e \approx 0.7$ MeV. Since the number of electrons is equal to that of ions ($Z = 1$), electrons must achieve, on the average, an energy of the order of that required for the ions, that is 6 MeV. The situation can be described by saying the each electron must receive about 8.6 "kicks" with energy equal to the quiver one. The average round trip for an electron in the plasma is estimated as $2R_0/c$ (c is the speed of light), so that, on average, each electron can see the laser field a number of times $t_{int}c/2R_0 = c/V_i \approx 13$.

In the previously dimensioned system, the electronic motion is practically collisionless, and ions can take energy by electrostatic coupling during the system expansion. Consistent with the previous scheme, global, forward collimation effects due to transfer of electromagnetic momentum are expected to be negligible. Actually a simple estimate shows that

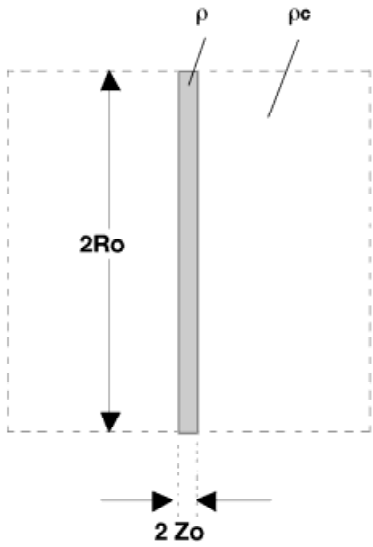

Fig. 16. The exploding foil geometry.

https://doi.org/10.1017/S0263034601192190 Published online by Cambridge University Press

$$\frac{\Delta V_i}{V_i} \approx \frac{1}{2}\left(\frac{2}{\eta_{abs}} - 1\right)\frac{V_i}{c}, \tag{13}$$

where ΔV_i is the additional velocity due to radiation pressure. For $V_i \approx 2.4 \times 10^9$ cm/s and $\eta_{abs} = 0.5$, $\Delta V_i / V_i \approx 0.12$. However, for $\eta_{abs} = 0.08$, it is found that $\Delta V_i / V_i \approx 1$. In practice, the effect is substantial when the energy transfer is inefficient. More effective can be the mechanism of collimation by pressure gradient. Since the gradient of pressure is greater in the direction normal to the thin foil surface, a bilateral collimation effect can result for thin foils. The asymptotic value of the F/Number can be numerically found by integrating the fluid equations for a 2-D, Gaussian density distribution representing initially cold foils with cylindrical symmetry. In our calculations, an inner power source representing the energy given by the laser to the electrons started the hydrodynamic motion. The duration of the energy source in units of the explosion time t_{expl} was taken in the ratio $(R_0/Z_0)^{2/3}$, according to the prescription given by Eq. 9. The results of these calculations are represented in Figure 17, where the F/Number is given as function of the foil aspect ratio. It is seen that for the aspect ratios of interest (20–50) F/Number in excess of 2 are possible.

In the previous considerations, a framing of the global behavior of the exploding foil was tried. The individuated regime is quite different from those studied in experiments up to now. The distinctive feature is the long duration of the pulse (≈15–20 ps) associated to high intensity (possibly $1–5 \times 10^{18}$ W/cm^2). For these power densities, theory and experiments normally consider 0.5–1 ps duration (see Berg *et al.*, 1997 and Key *et al.*, 1999). Moreover, to reach high power density in the experiments, the pulse energy was deposited in spots around 10 μm wide, a few light wavelengths. In the case here considered, systems with diameters several 100 μm wide are assumed and the target substantially expands during the interaction. Key information for the application of thin-foil explosion to an usable production of LIB is related to the value of η_{abs} and to the way the absorbed energy is shared between the foil particles. For instance, a small value of η_{abs} would affect the efficiency of the method. The self-organization of a fraction of the plasma in high-energy jets during the interaction could have the same effect or, at least, would imply changes in the model to be used for foil dimensioning.

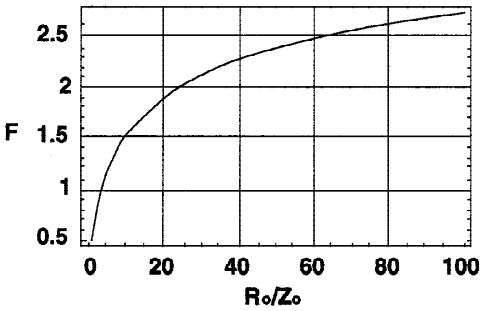

Fig. 17. The asymptotic F/Number for exploding Gaussian thin foils as function of the foil aspect ratio.

6. IMPLOSION SCALING

The simulations presented for IE in the previous sections have been made for reactor-sized targets. However, by theoretical scaling (Caruso & Strangio, 1999), it is possible to deduce the parameters for implosions having similar performances in terms of *gain*, *hydrodynamics*, *driver*, and *α-particle transport*. As functions of the initial implosion energy (E), the target and the parameters of the pulse ought to be scaled, in geometrical similarity, as follows. *Size* $\propto E^{1/2}$; *density* $\propto 1/E^{1/2}$; *ignition driver energy* $\propto E$; *ignition driver pulse duration* $\propto E^{1/2}$; *implosion velocity* unchanged. The ignition driver has to be modeled in such a way to keep constant the quantity *density* × *material-opacity* × *size*, at material temperature unchanged. The associated on-target power density ought to scale as: *power density* $\propto E^{-1/2}$. For the cases considered in this paper, it is sufficient to keep the HIB or the LIB ionic energy constant, or to change the X-ray *beam frequencies* according to $\propto 1/E^{1/6}$ (free-free opacity). Being that the gain (fusion energy/E) is a pure number, similarity for gain simply means that the gain remains the same. The previous analytical scaling rules have been checked successfully by 2-D numerical simulations. The code (see Sect. 1) includes a more complete physical description than that used to deduce the scaling. The quality of the scaling can be appreciated from the results of simulations shown in Figures 18 and 19. The comparison is made between two targets, the reference one (RT) and the scaled one (ST).

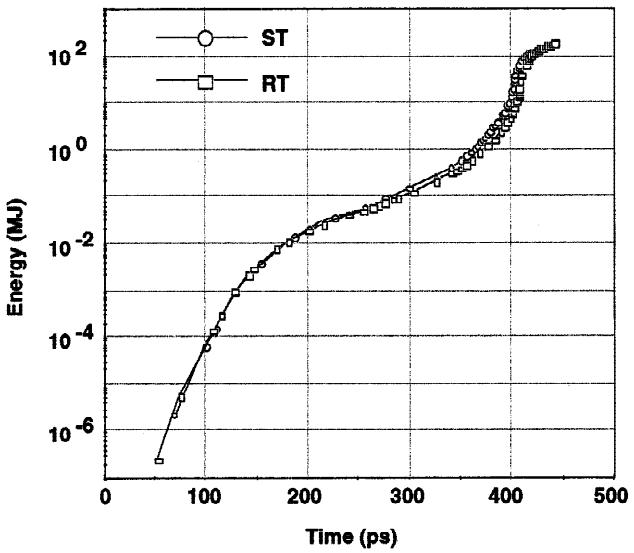

Fig. 18. Thermonuclear burn of ST and RT. To design ST, the RT energy values were down-scaled by 0.2. The corresponding times were scaled by a factor $0.2^{1/2}$, according to the theoretical scaling. With respect to the RT target data, at intermediate burn, the ST data result shifted to the left by about 10 ps.

https://doi.org/10.1017/S0263034601192190 Published online by Cambridge University Press

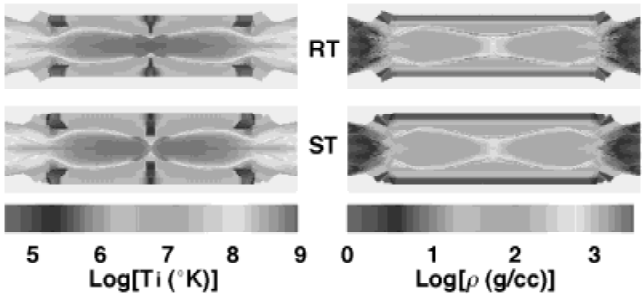

Fig. 19. Comparison of ionic temperature and density for ST and RT targets. The implosion energy for ST was 0.2 that of RT. The frames are taken at corresponding times, according to the theoretical scaling. RT coordinates, density, and temperature are also reduced accordingly.

Both RT and ST were ignited by X-ray two-sided irradiation. RT was a reactor-sized target producing, after burn quenching, more than 2000 MJ. The target parameters of RT were those indicated in column 1 of Table 1. The X-ray pulse duration, t_{dr2}, was 450 ps and its spectral distribution was that described in the previous section. ST parameters and its IE driver were deduced by the previous scaling, for E reduced by a factor 0.2. Downscaled designs could be useful for high-gain test experiments.

7. CONCLUSIONS

It has been shown that ignition and high-burn can be obtained from imploding finite-length cylinders ignited in the injected entropy mode (IE). This sort of assisted ignition for imploding targets presents several advantages. If compared to the standard, totally self-generated spark method, the EI approach promises substantial relaxation of the implosion quality requirements. Compared to fast ignition, the IE method implies the use of less performing drivers.

The method was discussed for different ignition-assisting energy vectors, such as heavy-ion beams, light-ion beams, and soft X-rays. Some of the issues associated to these assisting drivers have been also considered.

In the cases presented in this paper, ignition was localized in the center or near one of the cylinder ends, so that most of the fuel in the imploding system represented the payload. In this regard cylindrical implosions present the possibility for tailoring the implosion story along the cylinder axis, to increase the gain. For instance, if a cold implosion at velocity of 3×10^7 cm/s is needed in the portion of cylinder where the ignition spark has to be formed, a lower velocity cold implosion can be used in the payload, where the burn propagates. This is important because 3×10^7 cm/s correspond to a kinetic energy of 0.045 MJ/mg, whereas (e.g.) 0.01 MJ/mg are needed to compress a cold fuel at 400 g/cm^3.

REFERENCES

Afanasiev, Yu.V. *et al.* (1975). *JETP Lett.* **21** (2), 68.
Basov, N.G. *et al.* (1992). *Sov. Laser Res.* **13** (5), 396.
Berg, F.N. *et al.* (1997). *Phys. Plasmas* **4**(2), 447.
Brueckner, K.A. *et al.* (1982). *Phys. Rev. B* **25**, 4377.
Callahan, D.A. & Langdon, A.B. (1996). *LLNL ICF Quarterly Report,* **6** (3), p. 89.
Caruso, A. (1994). Proceedings IAEA Technical Committee Meeting on Drivers for Inertial Fusion, Paris, 14–18 November.
Caruso, A. & Gratton R. (1971). *Phys. Lett. A* **36**(4), 275.
Caruso, A. & Pais, V.A. (1996). *Nucl. Fusion* **36**(6), 745.
Caruso, A. & Pais, V.A. (1998). *Phys. Lett. A* **243**, 319.
Caruso, A. & Strangio, C. (1998). *JETP* **86**(3), 439.
Caruso, A. & Strangio, C. (1999). *IFSA Proceedings*, p. 88.
Caruso, A. & Strangio, C. (2000). *Laser Part. Beams* **18**, 1–13.
Key, M.H. *et al.* (1999). *IFSA 99 Proceedings and Preprint UCRL-JC-135477,* p. 392.
Kirkpatrick, R.C. (1979). *Nucl. Fusion* **19**(1), 69.
Kirkpatrick, R.C. & Wheeler, J.A. (1981). *Nucl. Fusion* **21**(3), 389.
Lindl, J. (1995). *Phys. Plasmas* **2**(11), 3933.
Los Alamos EOS and Opacity Group (1983). LANL Report LALP-83-4.
Mehlhorn, T.A. (1981). *Journal of Applied Physics* **52**, 6522.
Nuckolls, J.H. *et al.* (1972). *Nature* **239**, 129.
Pais, V.A. & Caruso, A. (1990). *Comp. Phys. Commun.* **58**, 55.
Tabak, M. *et al.* (1994). *Phys. Plasmas* **1**(5), 1626.

https://doi.org/10.1017/S0263034601192190 Published online by Cambridge University Press